Available online at www.sciencedirect.com
ScienceDirect
Agricultural and Forest Meteorology 139 (2006) 55–73
AGRICULTURAL AND FOREST METEOROLOGY
www.elsevier.com/locate/agrformet

Analytical integrated functions for daily solar radiation on slopes

Richard G. Allen *, Ricardo Trezza, Masahiro Tasumi

University of Idaho Research and Extension Center, Kimberly, ID, United States

Received 24 November 2005; accepted 19 May 2006

Abstract

This paper presents a procedure for estimating daily global solar radiation for inclined surfaces having specified slope and aspect for application with surface energy balance models for determining evapotranspiration. Procedures are provided for developing clear sky solar curves and for translating measured solar radiation from a horizontal surface to slopes. The procedure assumes an extensive surface having uniform slope at each point of calculation, so effects of protruding surrounding terrain are not considered. This simplification of terrain aids the application of the procedure within image processing models used for surface energy balance and evapotranspiration calculations, allows the use of a purely analytical solution, which is useful for some types of software, and provides sufficiently accurate results for terrain having gradual to moderate changes in slope. Extraterrestrial solar radiation is computed using an analytical solution for 24-h periods. New developments reported here include a detailed procedure for determining integration limits for the analytical solution that applies to all combinations of slope, aspect and latitude, including steep polar facing slopes where the sun may appear twice per day. Use of clear sky transmissivity procedures from ASCE-EWRI that calculate direct beam and diffuse radiation components separately as a function of elevation, sun angle and precipitable water reduces or eliminates the need for local calibration. Other developments include an improved function describing the reduction in hemispherical diffuse radiation with slope and adjustment of mean daily beam transmissivity using a weighted mean daily solar elevation. Simulated clear sky solar radiation envelope curves and translated measured solar radiation compare well with measurements from two locations in the U.S. over a range of slope and aspect.

Keywords: Solar radiation; Clear-sky solar radiation; Slope; Terrain; Diffuse radiation; Translation

1. Introduction

The amount of solar radiation received by a given surface is controlled, at the global scale, by the geometry of the earth, atmospheric transmittance, and the relative location of the sun. At the local scale, radiation is additionally controlled by surface slope, aspect and elevation. Estimation of clear sky solar radiation for sloped surfaces is important in remote sensing applications involving energy balance and ET estimation, which need an estimation of total energy striking a given surface. Most solar radiation (R_S) information comes from weather stations located in flat areas, so that estimation of R_S in sloped surfaces is generally based on models. On inclined surfaces, the total (global) radiation reaching the surface consists of the sum of three components: direct (beam) radiation, which is the part of solar radiation that is not absorbed or scattered by the atmosphere and that reaches the surface directly from the sun; diffuse radiation, which

* Corresponding author. Fax: +1 208 423 6559.
E-mail addresses: rallen@kimberly.uidaho.edu (R.G. Allen), rtrezza@kimberly.uidaho.edu (R. Trezza), tasumi@kimberly.uidaho.edu (M. Tasumi).

0168-1923/$ – see front matter
doi:10.1016/j.agrformet.2006.05.012

originates from the solar beam, but is scattered toward the surface; finally, a relatively small component of radiation reflected from ground surfaces in view of the inclined surface that becomes incident to the inclined surface in diffuse form. This component is modeled as hemispherical reflected radiation from a horizontal surface lying below the incline.

The calculation methodology described here builds on previous analytical models by Revfeim (1978) and Tian et al. (2001) by providing exact integration limits for 24-h periods that apply to all uniform slopes, aspects and latitudes and by developing 24-h clear sky solar radiation from extraterrestrial radiation utilizing a weighted sun elevation angle over the 24-h period for estimating direct and diffuse transmissivities. The methodology for estimating clear sky solar radiation does not require solar radiation measurements and applies to a wide-range of climates. The calculation methodology involves two steps: (1) calculation of extraterrestrial solar radiation (R_a) for a given combination of slope and aspect and (2) calculation of clear sky solar radiation from the extraterrestrial radiation. A third optional step involves the use of the developed functions to translate measured solar radiation, when available, to sloping surfaces. Calculation can be made for any instant or can be integrated over 24-h periods, so that the functions for developing clear sky from R_a and for translating R_S measurements can be applied with both numerical and analytical calculations for R_a. Numerical solutions of solar radiation models are now common and can be implemented in a wide range of programming and image processing environments. Most solar models using hourly or shorter timesteps are solved numerically. An analytical solution for solar radiation, as described in this article, is sometimes preferred over numerical solution, for example when non-iterative or non-looping algorithms are necessary for purposes of model qualification by government entities, where a sequential model procedure is amenable to description and solution in a report format, such as with some models and documents associated with the Yucca Mountain radioactive waste repository. Analytical solutions can be used to confirm numerical solutions and permit the translation of solar radiation measurements reported on a 24-h basis.

The procedure produces solar radiation estimates that are generally within the uncertainty of surface energy balance and evapotranspiration estimation procedures. A benefit of the procedure is that no local or regional calibration is required. The simplification of the terrain via the assumption of uniform extensive slopes, without considering the possibility of cast shading, might lead to some gross errors in cases of rough terrain. For example, in very rough terrain, some areas may not receive any direct radiation during the whole year, even if facing south because of high obstacles surrounding them. The effect of obstacles is largest during periods of low sun. These extreme examples are rare but may be important in some applications. Under these conditions, GIS-based solar models that consider impacts of terrain shading, such as by Flint and Childs (1987) and Fu and Rich (1999), are recommended.

2. 24-h extraterrestrial solar radiation

Extraterrestrial solar radiation at any instant of time during daylight is a function of solar incidence angle:

$$R_a = \frac{G_{SC} \cos\theta}{d^2} \tag{1}$$

where G_{SC} is the solar constant (1367 W m^{-2}), d the relative earth–sun distance in astronomical units, and $\cos\theta$ is the cosine of the solar incidence angle relative to the normal to the land surface. The land surface is assumed to be represented by a plane having slope s and aspect γ.

Parameter d^2 is a function of day of year and can be calculated using Duffie and Beckman (1991):

$$d^2 = \frac{1}{1 + 0.033\cos\left(\frac{\mathrm{DOY}2\pi}{365}\right)} \tag{2}$$

where DOY is day of year and (DOY2π/365) is in radians.

A full equation for computing the instantaneous angle of incidence for beam radiation on sloping surfaces is taken from Garner and Ohmura (1968) and Duffie and Beckman (1980):

$$\begin{aligned}\cos\theta = {} & \sin(\delta)\sin(\phi)\cos(s) \\ & - \sin(\delta)\cos(\phi)\sin(s)\cos(\gamma) \\ & + \cos(\delta)\cos(\phi)\cos(s)\cos(\omega) \\ & + \cos(\delta)\sin(\phi)\sin(s)\cos(\gamma)\cos(\omega) \\ & + \cos(\delta)\sin(\gamma)\sin(s)\sin(\omega)\end{aligned} \tag{3}$$

where δ is the declination of the earth (positive during northern hemisphere summer), ϕ the latitude of the pixel (positive for the northern hemisphere and negative for the southern hemisphere), s the surface slope, where $s = 0$ for horizontal and $s = \pi/2$ radians for vertical slope (s is always positive and represents the slope in any

direction), and γ is the surface aspect angle, where $\gamma = 0$ for slopes oriented due south, $\gamma = -\pi/2$ radians for slopes oriented due east, $\gamma = +\pi/2$ radians for slopes oriented due west and $\gamma = \pm\pi$ radians for slopes oriented due north. Parameter ω is the hour angle, where $\omega = 0$ at solar noon, ω is negative in morning and ω is positive in afternoon. When applying (3) for an instant in time (i.e., for numerical-based solutions), ω deviates from local time according to seasonal correction for time given, for example, by Duffie and Beckman (1980, 1991) and repeated by ASCE-EWRI (2005).

For applications to strictly horizontal land surfaces, where slope is zero and aspect is not relevant, Eq. (3) reduces to:

$$\cos\theta_{\text{hor}} = \sin(\delta)\sin(\phi) + \cos(\delta)\cos(\phi)\cos(\omega) \tag{4}$$

where $\cos\theta_{\text{hor}}$ is the cosine of the solar incidence angle relative to the normal to a horizontal surface. Eq. (3) can be integrated between two daytime sun-hour angles, ω_1 and ω_2, to provide total extraterrestrial radiation during the period when used with Eq. (1):

$$\begin{aligned}\int_{\omega_1}^{\omega_2} \cos(\theta)\,\mathrm{d}\omega &= \sin(\delta)\sin(\phi)\cos(s)(\omega_2-\omega_1)\\ &\quad - \sin(\delta)\cos(\phi)\sin(s)\cos(\gamma)(\omega_2-\omega_1)\\ &\quad + \cos(\delta)\cos(\phi)\cos(s)(\sin(\omega_2)-\sin(\omega_1))\\ &\quad + \cos(\delta)\sin(\phi)\sin(s)\cos(\gamma)(\sin(\omega_2)-\sin(\omega_1))\\ &\quad - \cos(\delta)\sin(s)\sin(\gamma)(\cos(\omega_2)-\cos(\omega_1))\end{aligned} \tag{5}$$

When ω_1 and ω_2 of Eq. (5) are set equal to $\omega_{1_{24}}$ and $\omega_{2_{24}}$, defined as the beginning and ending sun-hour angles when the sun's beam first and last strikes the particular surface, the associated equation for 24-h extraterrestrial radiation, $R_{a_{24}}$, is:

$$R_{a_{24}} = \frac{G_{SC}}{d^2}\int_{\omega_{1_{24}}}^{\omega_{2_{24}}} \cos(\theta)\,\mathrm{d}\omega \tag{6}$$

where the integral is computed using (5) with limits $\omega_{1_{24}}$ and $\omega_{2_{24}}$. The solar beam angle is assumed to originate from the center of the solar disk. This assumption causes little error in 24-h estimates of solar radiation because radiation intensity normal to the earth's surface is low during at least one of the integration limits. Use of the center of the disk approximates for partial disk visibility for some minutes after the center of the disk appears. Some diffuse radiation, described later, occurs prior to visibility of the sun's disk. However, this radiation amount is very small relative to daily total solar radiation, generally being less than 0.1%.

2.1. Two periods of beam radiation within a day

The integration of Eq. (5) and application of Eq. (6) presume that there is a single, continuous direct beam period during the day. In areas having steep slopes away from the sun, one must identify situations where the sun beam strikes the surface during two separate portions of the day. This situation can occur on relatively steep slopes facing away from the noontime sun during summer. In these situations, the slope may see the sun at sunrise, but then have the sun disappear behind the slope during midday, and then reappear before final sunset

To test whether a situation of two periods of direct beam radiation can potentially occur, the following Eq. (7) is solved, and if true, then the slope exceeds the solar angle at solar noon and the possibility exists for two periods of direct beam radiation:

$$\sin s > \sin\phi\cos\delta + \cos\phi\sin\delta \tag{7}$$

If Eq. (7) is true, then the sequence of conditionals described in Appendix A, step D, should be applied to confirm that midday shading does occur so that two sets of integrations can be calculated and applied. These types of integration limits have not been reported elsewhere.

For a horizontal surface, $\omega_{1_{24}}$ and $\omega_{2_{24}}$ are equal to $-\omega_S$ and ω_S, where $-\omega_S$ is sunrise time angle and ω_S is the sunset time angle calculated as:

$$\omega_S = \arccos(-\tan(\delta)\tan(\phi)) \tag{8}$$

where, by definition, $\omega = 0$ at solar noon.

2.2. General integration limits for Eq. (5)

The following integration limit procedure presumes that the slope extends in all directions. This presumption allows the application of the analytical solution to calculate 24-h extraterrestrial and short wave radiation. Some approaches have used discretized elevation maps to locate maximum terrain angles for complex terrain (Swift, 1976; Dubayah et al., 1990; Varley et al., 1996). However, these latter applications require numerical integration of (3) and the use of a special spatial database and processor. The simplification of terrain aids in application within image processing models and spreadsheets used for surface energy balance and evapotranspiration calculation, since only a single cell within an image needs to be processed, and provides sufficiently accurate results for these types of applica-

tions. Single cell processing can be important with some types of satellite images such as Landsat that contain more than 25 million cells.

For many slopes, the sun-hour angle where the solar beam first strikes or last strikes the slope occurs when $\cos(\theta) = 0$. For a sloping surface facing away from sunrise or facing away from sunset, $\cos(\theta) = 0$ occurs after sunrise or prior to sunset. For a sloping surface facing toward the sunrise, the sun-hour angle where the solar beam first strikes the slope is when $\omega = -\omega_S$. In this situation $\cos(\theta) \neq 0$ at the initiation of solar beam incidence to the slope. For a sloping surface facing toward the sunset, the sun-hour angle where the solar beam last strikes the slope is when $\omega = \omega_S$.

For situations where the slope faces away from the sun at horizontal sunrise or away from the sun at horizontal sunset (3), can be solved for $\cos(\omega)$, given $\cos(\theta) = 0$ to find the potential integration limits for the day:

$$\cos(\omega) = \frac{\begin{array}{l}\sin(\delta)\cos(\phi)\sin(s)\cos(\gamma) - \sin(\delta)\sin(\phi)\cos(s) \\ -\cos(\delta)\sin(s)\sin(\gamma)\sin(\omega)\end{array}}{\cos(\delta)\cos(\phi)\cos(s) + \cos(\delta)\sin(\phi)\sin(s)\cos(\gamma)} \tag{9}$$

Eq. (9) has ω on both the left hand and right hand sides and can be re-expressed as:

$$\cos(\omega) = \frac{a}{b} - \frac{c}{b}\sin(\omega) \tag{10}$$

where a, b, and c are constants for a given day, latitude, slope and slope azimuth:

$$a = \sin(\delta)\cos(\phi)\sin(s)\cos(\gamma) - \sin(\delta)\sin(\phi)\cos(s) \tag{11a}$$

$$b = \cos(\delta)\cos(\phi)\cos(s) + \cos(\delta)\sin(\phi)\sin(s)\cos(\gamma) \tag{11b}$$

$$c = \cos(\delta)\sin(s)\sin(\gamma) \tag{11c}$$

Squaring both sides of (10) and solving for $\sin(\omega)$ using the quadratic solution:

$$\sin(\omega) = \frac{\frac{2ac}{b^2} \pm \sqrt{\left(\frac{2ac}{b^2}\right)^2 - 4\left(1 + \frac{c^2}{b^2}\right)\left(\frac{a^2}{b^2} - 1\right)}}{2\left(1 + \frac{c^2}{b^2}\right)} \tag{12}$$

Both solutions from (12) are useful, as they potentially represent the times of sunrise and sunset for the sloping surface. The preliminary predictions to $\sin(\omega)$, simplified by canceling of common terms, are:

$$\sin(\omega_{1_{24}}) = \frac{ac - b\sqrt{b^2 + c^2 - a^2}}{b^2 + c^2} \tag{13a}$$

$$\sin(\omega_{2_{24}}) = \frac{ac + b\sqrt{b^2 + c^2 - a^2}}{b^2 + c^2} \tag{13b}$$

where $\omega_{1_{24}}$ and $\omega_{2_{24}}$ are candidate values for sunrise and sunset hour angles for use as limits in Eq. (6). These limits are valid if there is only a single period of beam radiation in a 24-h period. This is generally valid for west, south and east facing slopes (in the northern hemisphere). Eq. (13) has similar form to solutions by Klein (1977) and Duffie and Beckman (1980, 1991), but can be used in association with Appendix A to determine multiple integration limits for when the sun strikes twice per day or to determine when there is no beam radiation on a steep surface during fall and winter. In application of (13a) and (13b), the expression under the radical must be limited to non-negative values.

During solution of (13), an efficient recalculation of (3) is possible using variables a, b, and c from (11), if previously calculated:

$$\cos(\theta) = -a + b\cos(\omega) + c\sin(\omega) \tag{14}$$

Eq. (14) is equivalent to Eq. (3).

2.2.1. Refinement to the integration limits

Appendix A refines integration limits to Eq. (5) derived initially from Eq. (13) so that they correctly apply for all combinations of slope, aspect and latitude. These refinements were not utilized in previous models of Klein (1977), Revfeim (1978), Tian et al. (2001), and Duffie and Beckman (1980). The calculations for integration limits from (13a) and (13b) serve as candidate limits for $\omega_{1_{24}}$ and $\omega_{2_{24}}$. However, two angles ω_1 may exist that have the same $\sin(\omega_1)$ value. This occurs because ω is defined as $\omega = 0$ when facing due south in the northern hemisphere. Therefore, two solar angles can exist, one north of east and one south of east that have the same $\sin(\omega_1)$ value, but different value for ω_1. The same applies for ω_2. Therefore, a search must be performed using (3) and ω_S to determine the correct value for $\omega_{1_{24}}$ and $\omega_{2_{24}}$. In addition, two periods of direct beam radiation can occur per day for pole facing slopes where Eq. (7) is true. Appendix A describes the solution for the two sets of integration limits necessary to determine 24-h total extraterrestrial radiation, as described in Appendix A.

3. Calculation of clear-sky solar radiation

Clear sky solar radiation, R_{so} (W m^{-2}) is often simulated as:

$$R_{so} = R_a \tau_{swo} \tag{15}$$

where R_a is extraterrestrial solar radiation (W m^{-2}) and τ_{swo} is the broadband atmospheric transmissivity for shortwave radiation for cloud-free conditions (dimensionless).

Allen (1996) presented an approach for τ_{swo} and later updated in ASCE-EWRI (2005) that does not generally require local calibration or local coefficients. The methodology separately calculates transmissivity for direct beam and diffuse radiation:

$$\tau_{swo} = \frac{R_{so}}{R_a} = K_{Bo} + K_{Do} \tag{16}$$

where K_{Bo} is the clearness index for direct beam radiation for cloudless conditions and K_{Do} is the index for diffuse beam radiation. K_{Bo} is calculated in ASCE-EWRI (2005) considering the effects of sun angle, elevation and water vapor on the effective optical mass of the atmosphere impacting the absorption or scattering of short wave radiation as:

$$K_{Bo} = 0.98 \exp\left[\frac{-0.00146P}{K_t \sin\beta} - 0.075\left(\frac{W}{\sin\beta}\right)^{0.4}\right] \tag{17}$$

where K_t is an empirical turbidity coefficient, $0 < K_t \leq 1.0$ where $K_t = 1.0$ for clean air (typical of regions of agricultural and natural vegetation) and $K_t = 0.5$ for extremely turbid, dusty or polluted air, P the atmospheric pressure (kPa) computed as a function of elevation, β the angle of the sun above the horizon (radians), and W is the equivalent depth of precipitable water in the atmosphere (mm). The form of Eq. (17) stems from Majumdar et al. (1972), with coefficients updated by ASCE-EWRI (2005) for application across the U.S. W is computed in the ASCE-EWRI (2005) procedure following Garrison and Adler (1990) as:

$$W = 0.14 e_a P + 2.1 \tag{18}$$

where e_a is actual vapor pressure (kPa).

The diffuse radiation index $K_{Do_{hor}}$ under clear sky or near clear sky conditions is defined as $K_{Do_{hor}} = R_{Do_{hor}}/R_a$, where $R_{Do_{hor}}$ is diffuse clear sky radiation on a horizontal surface. $K_{Do_{hor}}$ is computed by ASCE-EWRI (2005) as a function of the direct beam coefficient using relationships developed by Boes (1981), but with coefficients determined by ASCE-EWRI based on 49 locations across the U.S. The ASCE-EWRI relationship is expressed in three parts:

$$K_{Do_{hor}} = 0.35 - 0.36 K_{Bo_{hor}} \quad \text{for } K_{Bo_{hor}} \geq 0.15 \tag{19a}$$

$$K_{Do_{hor}} = 0.18 + 0.82 K_{Bo_{hor}} \quad \text{for } 0.065 < K_{Bo_{hor}} < 0.15 \tag{19b}$$

$$K_{Do_{hor}} = 0.10 + 2.08 K_{Bo_{hor}} \quad \text{for } K_{Bo_{hor}} \leq 0.065 \tag{19c}$$

where $K_{Bo_{hor}}$ is a clearness index that is set equal to K_{Bo} from Eq. (17) when estimating for cloudless conditions and using $\sin\beta$ defined for a horizontal surface. Eq. (19) applies to both cloud-free and cloudy conditions; however, its accuracy is highest for estimating clear or nearly clear sky conditions. A combined function including Eq. (19a) and a function by Vignola and McDaniels (1986) is presented later for estimating K_D under both clear and cloudy conditions. Eq. (19) agrees well with data from Liu and Jordan (1960) as well as Boes (1981) and data by University of Oregon (2005), and provides a general estimation of diffuse radiation for the U.S. Eqs. (17)–(19) are generally valid for instantaneous or short timesteps (i.e., for use in numerical-based solutions) and for 24-h timesteps (for use in analytical solutions) (Allen, 1996; ASCE-EWRI, 2005).

For instantaneous calculations, sun angle β above the horizontal is calculated as:

$$\sin\beta = \sin\phi \sin\delta + \cos\phi \cos\delta \cos\omega \tag{20}$$

For daily (24-h) time periods, the average value of $\sin\beta$, weighted according to R_a, is calculated by integrating the product of solar elevation above a horizontal surface (to represent beam path length) (Eq. (20)) and solar intensity on an inclined surface, as represented by $\cos\theta$ (Eq. (3)). The weighted average $\sin\beta$ is required in Eq. (17) to improve accuracy of the K_{Bo} estimate when applied to 24-h periods, as this represents the mean relative path length through the atmosphere. The integration is performed over the day where limits ω_1 and ω_2 represent the beginning and ending of the daylight period as previously defined:

$$\sin\beta_{24} = \frac{\int_{\omega_{1_{24}}}^{\omega_{2_{24}}} (-a + b\cos(\omega) + c\sin(\omega))(\sin(\delta)\sin(\phi) + \cos(\delta)\cos(\phi)\cos(\omega))\,d\omega}{\int_{\omega_{1_{24}}}^{\omega_{2_{24}}} (-a + b\cos(\omega) + c\sin(\omega))\,d\omega} \tag{21}$$

Table 1
Definitions of parameters f_1–f_5 for use in Eq. (22) (limits $\omega_{1_{24}}$, $\omega_{2_{24}}$ are as defined in the previous section on computing cos θ and limits $\omega_{1_{24a}}$ and $\omega_{1_{24b}}$ are developed in Appendix A)

Parameter	Formula for 'f' parameter for one integration period per day	Formula for 'f' parameter for two integration periods per day using limits from Appendix A
f_1	$\sin(\omega_{2_{24}}) - \sin(\omega_{1_{24}})$	$\sin(\omega_{2_{24b}}) - \sin(\omega_{1_{24}}) + \sin(\omega_{2_{24}}) - \sin(\omega_{1_{24b}})$
f_2	$\cos(\omega_{2_{24}}) - \cos(\omega_{1_{24}})$	$\cos(\omega_{2_{24b}}) - \cos(\omega_{1_{24}}) + \cos(\omega_{2_{24}}) - \cos(\omega_{1_{24b}})$
f_3	$\omega_{2_{24}} - \omega_{1_{24}}$	$\omega_{2_{24b}} - \omega_{1_{24}} + \omega_{2_{24}} - \omega_{1_{24b}}$
f_4	$\sin(2\omega_{2_{24}}) - \sin(2\omega_{1_{24}})$	$\sin(2\omega_{2_{24b}}) - \sin(2\omega_{1_{24}}) + \sin(2\omega_{2_{24}}) - \sin(2\omega_{1_{24b}})$
f_5	$\sin^2(\omega_{2_{24}}) - \sin^2(\omega_{1_{24}})$	$\sin^2(\omega_{2_{24b}}) - \sin^2(\omega_{1_{24}}) + \sin^2(\omega_{2_{24}}) - \sin^2(\omega_{1_{24b}})$

Integration of (21) and combination of terms produces:

$$\sin\beta_{24} = \frac{[bg-ah]f_1 - cgf_2 + [0.5bh-ag]f_3 + 0.25bhf_4 + 0.5chf_5}{bf_1 - cf_2 - af_3} \quad (22)$$

with parameters f_1–f_5 defined in Table 1 and a–h defined in Table 2. Eq. (22) represents a complete integrated weighted average sin β for a 24-h period, where weighting is made according to potential solar intensity. Eq. (22) applies to any slope, aspect, latitude and time of year and is used to produce sin β_{24} to be used in place of sin β in Eq. (17) when applied to 24-h timesteps. The value for sin β_{24} should be limited to ≥ 0.

3.1. Clear sky radiation for horizontal surfaces

For horizontal areas (i.e., slope = 0), the 24-h clear sky solar radiation is calculated as:

$$R_{\mathrm{so}(24)_{\mathrm{hor}}} = \left\lfloor K_{\mathrm{Bo}(24)_{\mathrm{hor}}} + K_{\mathrm{Do}(24)_{\mathrm{hor}}} \right\rfloor R_{\mathrm{a}(24)_{\mathrm{hor}}} \quad (23)$$

where $R_{\mathrm{so}(24)_{\mathrm{hor}}}$ and $R_{\mathrm{a}(24)_{\mathrm{hor}}}$ are 24-h clear sky global and extraterrestrial solar radiation received on a horizontal surface, respectively. Units are typically expressed as average W m^{-2} of surface over the 24-h period. The direct beam and diffuse radiation components for 24-h periods on horizontal surfaces under clear sky conditions ($R_{\mathrm{Bo}(24)_{\mathrm{hor}}}$ and $R_{\mathrm{Do}(24)_{\mathrm{hor}}}$) are separately:

$$R_{\mathrm{Bo}(24)_{\mathrm{hor}}} = K_{\mathrm{Bo}(24)_{\mathrm{hor}}} R_{\mathrm{a}(24)_{\mathrm{hor}}} \quad (24)$$

$$R_{\mathrm{Do}(24)_{\mathrm{hor}}} = K_{\mathrm{Do}(24)_{\mathrm{hor}}} R_{\mathrm{a}(24)_{\mathrm{hor}}} \quad (25)$$

where $K_{\mathrm{Bo}(24)_{\mathrm{hor}}}$ and $K_{\mathrm{Do}(24)_{\mathrm{hor}}}$ are effective mean transmittances for direct beam (from Eq. (17)) and diffuse radiation (from Eq. (19)) over daylight periods for horizontal surfaces under clear sky. In calculation of $K_{\mathrm{Bo}(24)_{\mathrm{hor}}}$ using Eq. (17), the cos θ-weighted sin β_{24} calculation is simplified for the horizontal surface to:

$$\sin\beta_{24_{\mathrm{hor}}} = \frac{2g^2\omega_S + 4gh\sin(\omega_S) + h^2\left(\omega_S + \frac{1}{2}\sin(2\omega_S)\right)}{2(g\omega_S + h\sin(\omega_S))} \quad (26)$$

for horizontal surfaces, where

$$g = \sin(\delta)\sin(\phi) \quad (27)$$

$$h = \cos(\delta)\cos(\phi) \quad (28)$$

The numerator of Eq. (26) was derived by integrating $\cos^2\theta$ for horizontal surfaces, since cos θ serves as both the weight and as the direct equivalent of sin β when surfaces are horizontal.

Table 2
Equations for parameters a, b, c, g and h in Eq. (22)

$a = \sin(\delta)\cos(\phi)\sin(s)\cos(\gamma) - \sin(\delta)\sin(\phi)\cos(s)$
$b = \cos(\delta)\cos(\phi)\cos(s) + \cos(\delta)\sin(\phi)\sin(s)\cos(\gamma)$
$c = \cos(\delta)\sin(\gamma)\sin(s)$
$g = \sin(\delta)\sin(\phi)$
$h = \cos(\delta)\cos(\phi)$

3.2. Clear sky radiation for inclined surfaces

The solar radiation received on inclined surfaces is generally estimated by combining components of direct beam radiation, diffuse radiation, and radiation reflected toward the incline:

$$R_{\mathrm{so}(24)} = R_{\mathrm{Bo}(24)} + R_{\mathrm{Do}(24)} + R_{\mathrm{ro}(24)} \quad (29)$$

where $R_{\mathrm{so}(24)}$, $R_{\mathrm{Bo}(24)}$, $R_{\mathrm{Do}(24)}$, and $R_{\mathrm{ro}(24)}$ are the 24-h averages for global, direct, diffuse, and reflected solar radiation received by an inclined surface under clear

sky conditions. The magnitudes of components in (29) represent energy intensity at normal angles to the slope.

The direct component of global radiation received by the inclined surface is:

$$R_{\mathrm{Bo}(24)} = K_{\mathrm{Bo}(24)} R_{\mathrm{a}(24)} \tag{30}$$

where $K_{\mathrm{Bo}(24)}$ is 24-h effective beam transmittance for the inclined surface under cloudless conditions, and is calculated using Eq. (17), using Eq. (22) for $\sin(\beta_{24})$, where $\sin(\beta_{24})$ varies with slope and aspect.

The diffuse irradiance on an inclined surface under clear sky conditions is computed as some fraction or ratio, f_{ia}, of diffuse irradiance on a horizontal surface, $R_{\mathrm{Do}(24)_{\mathrm{hor}}}$:

$$R_{\mathrm{Do}(24)} = f_{\mathrm{ia}} R_{\mathrm{Do}(24)_{\mathrm{hor}}} \tag{31}$$

Models for predicting solar radiation generally differ in the calculation of diffuse sky radiation, due to the empiricism of estimation approaches (Perez et al., 1990). Diffuse models for slopes are commonly isotropic or anisotropic, where isotropic models assume diffuse radiation has the same intensity from all directions. Anisotropic models, such as those by Hay (1979), Reindl et al. (1990) and Perez et al. (1990) estimate different intensities of diffuse radiation from different regions of the atmosphere and relative to sun angle.

Isotropic approaches (Duffie and Beckman, 1980) estimate f_{ia}, known as the sky-view factor (Marks et al., 1979), as a simple function of the cosine of slope by setting $f_{\mathrm{ia}} = f_{\mathrm{i}}$ in Eq. (31), where $f_{\mathrm{i}} = (1 + \cos(s))/2$, stemming from integration of isotropic diffuse conditions over a vertical plane normal to the slope–horizontal interface. Revfeim (1978) showed that integration is more accurately made over a series of vertical planes having a variety of angles to the slope–horizontal interface. His solution for f_{i}, as presented in his Table 1, is well approximated as an average of the general cosine function and a simple linear function of slope as used, for example, by Tian et al. (2001) where $f_{\mathrm{i}} = (\pi - s)/\pi$, resulting in:

$$f_{\mathrm{i}} = \frac{\left(\frac{1+\cos(s)}{2} + \frac{\pi - s}{\pi}\right)}{2} = 0.75 + 0.25\cos(s) - \frac{0.5s}{\pi} \tag{32}$$

The assumption of isotropic diffuse radiation is reasonable when there is uniform cloud cover or when the atmosphere is hazy (Duffie and Beckman, 1991). For clear sky conditions, the assumption of an anisotropic behavior of diffuse radiation is considered to be more accurate (Perez et al., 1990; Hay, 1979; Reindl et al., 1990), where circumsolar enhancement of diffuse radiation in the vicinity of the sun and near the horizon is considered. Anisotropic models have been extensively used for predicting diffuse radiation on an hourly-basis (Perez et al., 1990; Reindl et al., 1990; Robledo and Soler, 1998; Diez et al., 2005) and a few applications using daily data have been reported (Collares-Pereira and Rabl, 1979, Hay, 1993; Nijmeh and Mamlook, 2000; Zeroual et al., 1996). In the case of anisotropic diffuse radiation, f_{ia} is calculated for clear sky conditions following Reindl et al. (1990):

$$f_{\mathrm{ia}} = (1 - K_{\mathrm{Bo}_{\mathrm{hor}}}) \times \left(1 + \left(\frac{K_{\mathrm{Bo}_{\mathrm{hor}}}}{K_{\mathrm{Bo}_{\mathrm{hor}}} + K_{\mathrm{Do}_{\mathrm{hor}}}}\right)^{0.5} \sin^3\left(\frac{s}{2}\right)\right) f_{\mathrm{i}} + f_{\mathrm{B}} K_{\mathrm{Bo}_{\mathrm{hor}}} \tag{33}$$

where f_{i} is from Eq. (32). Parameter f_{B}, the ratio of expected direct beam radiation on the slope to direct beam radiation on the horizontal surface, is calculated as:

$$f_{\mathrm{B}} = \frac{K_{\mathrm{Bo}}}{K_{\mathrm{Bo}_{\mathrm{hor}}}} \frac{R_{\mathrm{a}}}{R_{\mathrm{a}_{\mathrm{hor}}}} \tag{34}$$

where the inclusion of the ratio $K_{\mathrm{Bo}}/K_{\mathrm{Bo}_{\mathrm{hor}}}$ in the calculation of f_{B} is a new addition to represent differences in direct beam components caused by differences in mean solar elevation for the two projections. The ratio of direct beam transmissivity under cloudless conditions for the slope (K_{Bo}) to that for the horizontal ($K_{\mathrm{Bo}_{\mathrm{hor}}}$) is used to represent both cloudless and cloudy conditions for general application. K_{Bo} is calculated from Eq. (17) using $\sin\beta$ from (20) for instantaneous or from (22) for 24-h timesteps. $K_{\mathrm{Bo}_{\mathrm{hor}}}$ is calculated from Eq. (17) using $\sin\beta$ from (20) for instantaneous or from (26) for 24-h timesteps. The differences in $\sin\beta$ can vary between the two calculations, depending on slope and aspect. For instantaneous applications, the direct beam coefficients are equal and Eq. (34) reverts to expressions by Revfeim (1978) and Tian et al. (2001) that use only the ratio of extraterrestrial radiation on sloping and horizontal surfaces for 24-h timesteps and ignore the effects of differences in mean beam transmittance. R_{a} in (34) represents the extraterrestrial radiation on the slope for instantaneous or 24-h periods and is calculated from Eq. (1) using $\cos\theta$ from (3) for instantaneous and from Eq. (6) or (49) for 24-h periods. $R_{\mathrm{a}_{\mathrm{hor}}}$ represents the extraterrestrial radiation for a

horizontal surface for instantaneous or 24-h period and is calculated from Eq. (1) using cos θ from (4) for instantaneous and from Eq. (35) for 24-h periods. For 24-h periods:

$$R_{a_{hor24}} = \frac{G_{sc}}{\pi d^2}(\sin(\delta)\sin(\phi)\omega_S + \cos(\delta)\cos(\phi)\sin(\omega_S)) \quad (35)$$

Reflected radiance from surfaces in view of the inclined surface is estimated by assuming that both the beam and the diffuse radiation reflect isotropically from a horizontal surface at the foot of the inclined slope (Tian et al., 2001; Li et al., 2002; Duffie and Beckman, 1991). This is a reasonable and common assumption for unknown specific surface conditions at a point and at surrounding points, so that:

$$R_{ro(24)} = R_{so(24)hor}\alpha(1 - f_i) \quad (36)$$

where α is the average albedo of the surrounding ground surface below the inclined surface. Typical values for α are 0.15–0.25 for grasses, 0.10–0.15 for coniferous forest, 0.15–0.25 for deciduous forest, 0.04–0.08 for open water, and 0.15–0.35 for bare soil (Brutsaert, 1982). When measuring R_S on slopes where the sensor(s) is placed near the intersecting horizontal surface (i.e., within 10 m of the horizontal surface), any directional anisotropic reflectances from the horizontal surface will be manifested in the measurements and may cause deviation from R_{ro} modeled for extensive slopes (Ineichen et al., 1987).

Eq. (29) is applied for analytical solutions for 24 h timesteps. For numerical solutions having nearly instantaneous timesteps, R_{so} for a slope is calculated as:

$$R_{so} = K_{Bo}R_a + (f_{ia}K_{Do} + \alpha(1 - f_i)[K_{Bo} + K_{Do}])R_{a_{hor}} \quad (37)$$

where K_{Bo} is from (17) using sin β from (20), K_{Do} is from (19) using K_{Bo}, f_i is from (32), R_a is from (1) using (3) for cos θ and $R_{a_{hor}}$ is from (1) using (4) for cos θ. Parameters in (37) are solved at each instant in time or for small timesteps.

4. Translation of measured solar radiation from horizontal surfaces to slopes

Besides their use in estimating R_{so} representing clear sky conditions for sloping surfaces, the equations defining K_B and K_D can be used to translate measured R_S from horizontal surfaces (that measured by a leveled pyranometer) to sloping surfaces under both clear sky and cloudy conditions. This section describes the application of the general model of Revfeim (1978) as invoked by Tian et al. (2001) and other models (Reindl et al., 1990; Ineichen et al., 1990) to translate solar radiation measured from horizontal surfaces (i.e., weather stations) to sloping surfaces. The model by Revfeim is similar to Eq. (29) in that it assembles separate estimation or translation of direct beam, diffuse and reflected radiation into the equivalent solar radiation on a sloping surface (R_S):

$$R_S = R_{S_{mhor}}\left(f_B\frac{K_{B_{hor}}}{\tau_{sw_{hor}}} + f_{ia}\frac{K_{D_{hor}}}{\tau_{sw_{hor}}} + \alpha(1 - f_i)\right) \quad (38)$$

where $R_{S_{mhor}}$ is the measured global solar radiation on a horizontal surface, f_B the ratio of expected direct beam radiation on the slope to direct beam radiation on the horizontal surface, $K_{B_{hor}}$ the transmissivity index for actual direct beam radiation on the horizontal surface, $K_{D_{hor}}$ the index for actual diffuse radiation on the horizontal surface, and $\tau_{sw_{hor}}$ is the actual atmospheric transmissivity (direct + diffuse) for the horizontal surface. Eq. (38) applies to both cloudy and clear-sky conditions. $K_{B_{hor}}$, $K_{D_{hor}}$ and $\tau_{sw_{hor}}$ are all derived from the horizontal measurement. $\tau_{sw_{hor}}$ is calculated as:

$$\tau_{sw_{hor}} = \frac{R_{S_{mhor}}}{R_{a_{hor}}} \quad (39)$$

If the diffuse radiation component is considered to behave isotropically, $f_{ia} = f_i$. Otherwise, factor f_{ia} is calculated assuming anisotropic diffuse radiation similar to Reindl et al. (1990):

$$f_{ia} = (1 - K_{B_{hor}}) \times \left(1 + \left(\frac{K_{B_{hor}}}{K_{B_{hor}} + K_{D_{hor}}}\right)^{0.5}\sin^3\left(\frac{s}{2}\right)\right)f_i + f_B K_{B_{hor}} \quad (40)$$

Eq. (40) is the same as Eq. (33) except that $K_{B_{hor}}$ is used rather than $K_{Bo_{hor}}$. $K_{B_{hor}}$ is derived from the actual R_S measurement as a function of $\tau_{sw_{hor}}$ from Eq. (39) using a combined function based on Eq. (19a) for clear and partly cloudy conditions ($\tau_{sw_{hor}} > 0.42$) and a general function from Vignola and McDaniels (1986) for cloudy conditions:

$$K_{B_{hor}} = 1.56\tau_{sw_{hor}} - 0.55 \quad \text{for } \tau_{sw_{hor}} \geq 0.42 \quad (41a)$$

$$K_{B_{hor}} = 0.022 - 0.280\tau_{sw_{hor}} + 0.828\tau_{sw_{hor}}^2 + 0.765\tau_{sw_{hor}}^3 \quad \text{for } 0.175 < \tau_{sw_{hor}} < 0.42 \quad (41b)$$

$$K_{B_{hor}} = 0.016\tau_{sw_{hor}} \quad \text{for } \tau_{sw_{hor}} \leq 0.175 \quad (41c)$$

Eq. (19a) was re-expressed in (41a) on the basis of $\tau_{sw_{hor}}$. Trezza and Allen (2006) found Eq. (41b) and (41c) from Vignola and McDaniels to estimate diffuse radiation measured at the Desert Rock weather station in Nevada (NOAA-SURFRAD, 2006) more accurately than equivalent equations based on (19b) and (19c) under fully cloudy conditions ($\tau_{sw_{hor}} < 0.42$) (data not shown).

Parameter $K_{D_{hor}}$ is calculated as the difference between $\tau_{sw_{hor}}$ and $K_{B_{hor}}$:

$$K_{D_{hor}} = \tau_{sw_{hor}} - K_{B_{hor}} \quad (42)$$

Eqs. (41) and (42) apply well to both instantaneous and 24-h timesteps. Generally, 24-h timesteps are utilized in analytical processing models. The value for $\tau_{sw_{hor}}$ from Eq. (39) is sensitive to atmospheric pressure, which changes with elevation. Therefore, the theoretical value for f_B calculated from Eq. (34) may in reality be influenced by differences in K_{Bo} which may represent an elevation different from the location where $K_{Bo_{hor}}$ is determined. For instantaneous applications at the same elevation, the direct beam coefficients are equal and Eq. (34) reverts to expressions by Revfeim (1978) and Tian et al. (2001).

Parameters f_i and α in Eq. (40) have been previously defined. In numerical applications for translating 24-h R_S measurements to slopes, the day is divided into small discrete timesteps, for example, of 0.15 h in length, and f_B is calculated for each discretized time-step to account for effects of sun-angle on K_{Bo} and weighting with R_a. However, values for $\tau_{sw_{hor}}$, $K_{Bo_{hor}}$, and $K_{D_{hor}}$ in Eq. (38) are calculated only once for the 24-h period, based on the value for $R_{S_{mhor}}$ and Eqs. (41) and (42). The calculations from Eq. (38) for discretized steps are averaged over the 24-h period to produce 24-h average R_S for the sloped surface.

4.1. Equivalent solar radiation per horizontal area

The above calculations for R_S and R_{so} for sloping surfaces express radiation in W m^{-2} at a normal to the sloped surface. In energy balance work, including calculation of evapotranspiration, it is customary to reproject radiation and other energy balance components in terms of energy per horizontal equivalent for a defined calculation cell to be congruent with precipitation and other water balance terms. This is done for the computed R_S and R_{so} as:

$$R_{S_{equiv\_hor}} = \frac{R_S}{\cos(s)} \quad (43)$$

where R_S is solar radiation normal to the surface and s is the slope. The same calculation is done for R_{so}.

5. Testing of the analytical functions and limits for R_{so} and translation of measured R_S

Precision solar radiation data measured at two locations in the U.S. were applied to the described model for estimating extraterrestrial and solar radiation on inclined slopes under cloud-free conditions. The two stations described in Table 3 were selected based on rigorous calibration and quality control of the solar data. The Eugene, Oregon location is a low elevation site having dry summer and humid winter and the Golden, Colorado location is a high elevation site having dry summer and moderately dry, cold winter. Both of these

Table 3
Location information for precision solar radiation measurement sites

Station	Latitude (°)	Longitude (°)	Elevation (m)	Data used	Observation	Albedo used for surfaces[a]
Eugene, OR	44.0	−123.1	150	R_S horizontal	Pacific Northwest network,	–
				R_S 30° South facing	University of Oregon	0.20
				R_S 45° South facing		0.20
				R_S 90° South facing		0.05
				R_S 90° North facing		0.05
				Relative humidity		
				Air temperature		
Golden, CO	39.74	−105.18	1829	R_S horizontal	Solar Radiation Research	0.2 for all surfaces
				R_S 40° South facing	Laboratory (NREL)	(sparse grass, light soil)
				R_S 90° South facing		
				R_S 90° North facing		
				Relative humidity		
				Air temperature		

[a] Different surface albedos were used for difference sensors at Eugene due to the location of the sensors on a roof top comprised of varying material and to account for obstructions and shading of 90° sensors to reduce impacts of surface reflectance (Vignola, 2005, personal communication).

locations were equipped with solar pyranometers facing various directions and with various inclines. The Golden site was surrounded by natural vegetation and the Eugene site was on a flat roof top.

All measurements were made using Eppley precision spectral pyranometers (PSP) that measured total solar radiation (sum of direct and diffuse). Relative humidity and air temperature were used to estimate vapor pressure used in Eq. (18). All data were extracted from internet sites maintained by the University of Oregon and by the National Renewable Energy Laboratory.

6. Results

Fig. 1 shows extraterrestrial solar radiation (R_a), clear-sky R_{so} envelope, and measured R_S at Golden, CO, and Eugene OR for a horizontal surface. Each measurement point represents 24-h average radiation over 1 day expressed in W m^{-2}. The measured data that lay on or close to the R_{so} curve represent days having clear or mostly clear skies. The agreement of the data and the curve indicate good estimation by the R_{so} method for horizontal conditions and apparently good calibration of the pyranometer. In all applications, K_t in Eq. (17) was set equal to 1.0 (representing clear air having little haze). No calibration to any coefficients was done.

Figs. 2 and 3 show series of predicted clear-sky solar radiation envelopes derived from the developed equations and measured values of solar radiation for selected tilt angles (slopes) of sensors and south and north orientation (aspect) for the Colorado and Eugene locations. In general, maximum values of measured R_S corresponded well with the clear-sky conditions predicted by the R_{so} envelopes during all times of the year. The right-hand column of figures in Figs. 2 and 3 show actual R_S estimated using Eq. (35), where measured R_S on a horizontal surface (shown in Fig. 1) was translated into R_S for each of the slopes. Agreement between measured and predicted was very good for the south facing sensors (Fig. 2), with a similar population of data replicated.

In the case of the 90° north-facing aspects shown in Figs. 2 and 3, no solar beam struck the surface during fall and winter periods. Conversely, the beam struck the surface during two different periods during the day for days from DOY 81 to DOY 254 (spring and summer). This combination of vertical slope and north aspect represents an extreme condition where much, if not all, radiation incident to the surface is from diffuse and reflected sources. Total levels of radiation and differences are small relative to potential radiation on a horizontal surface, and results are considered to be relatively good. An interesting phenomenon for the steep north-facing slopes is that total solar radiation on cloudy days often exceeded the "clear-sky" R_{so} curve due to increased diffuse radiation on those days. This is opposite the situation for gentle slopes and for all slopes facing mostly south, where solar radiation on cloudy days is nearly always below the clear sky curve.

In Figs. 2 and 3, the translated R_S (estimated based on the horizontal measurements) generally followed the estimated R_{so} more closely than did the actual measured R_S on the incline because the translated R_S values were indexed to the R_{so} curves. $K_{B_{hor}}$ in the figures was estimated using Eq. (41).

Figs. 4–6 show scatter diagrams of translated (predicted from horizontal measurements) versus measured daily R_S for the series of slopes evaluated (the same data as plotted in Figs. 2 and 3). The scatter diagrams show relatively good agreement, with relatively low amounts of scatter about the 1:1 line. The translated R_S for the 90° south facing slope at Eugene exceeded measured R_S for that slope by about 10% and agreement for the 90° north-facing slopes, representing an extreme condition, had poorer agreement.

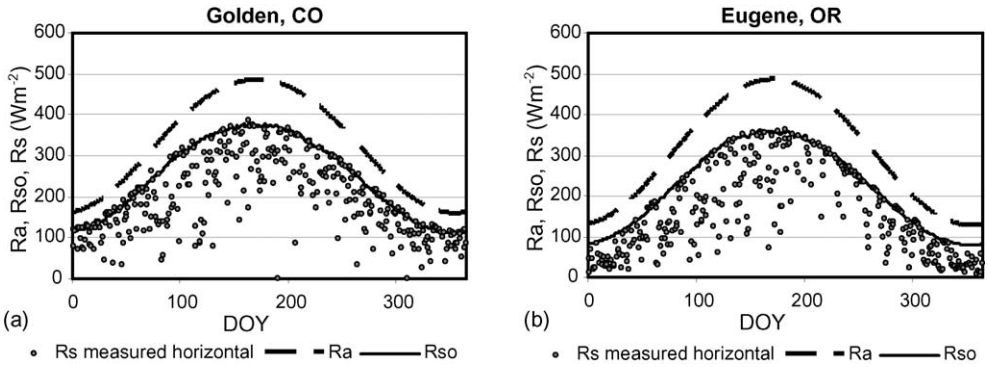

Fig. 1. Extraterrestrial solar radiation (R_a), clear-sky R_{so} envelope, and measured R_S at (a) Golden, CO, and (b) Eugene OR for a horizontal surface during 2002.

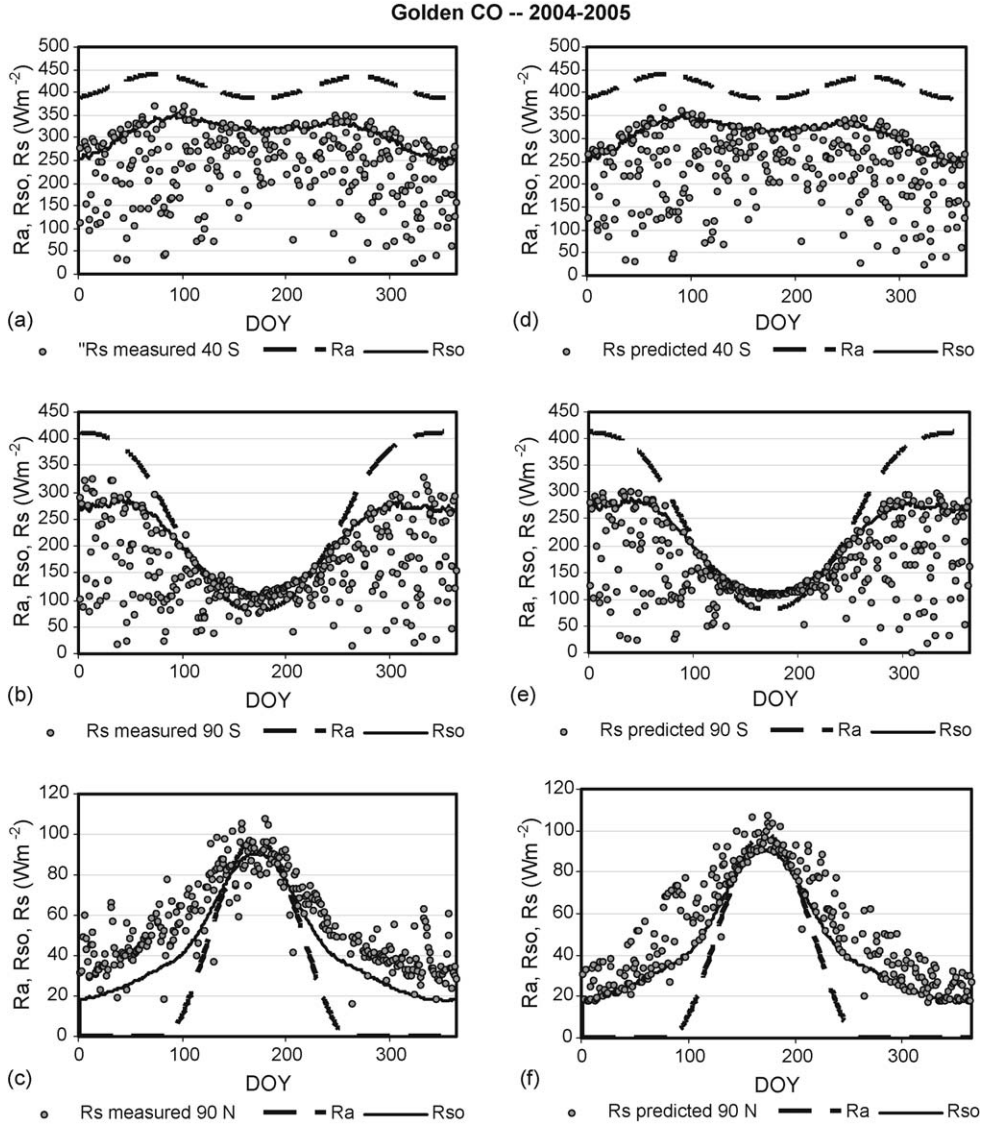

Fig. 2. Extraterrestrial solar radiation (R_a), clear-sky R_{so} envelopes, and measured R_S at Golden, Colorado corresponding to slopes of (a) 40° (south-facing), (b) 90° (south-facing) and (c) 90° (north-facing) and associated predicted R_S for (d) 40° (south-facing), (e) 90° (south-facing) and (f) 90° (north-facing) slopes.

Table 4 summarizes a statistical analysis of model performance for the data sets. Error parameters included the root mean square error (RMSE), mean absolute error (MAE), coefficient of efficiency (E) and modified index (d_i). These statistical indicators are defined in Appendix B. In general, error tended to be greater for higher slopes and for the north-facing aspect. For slopes of 30°, 40°, and 45°, MAE was less than 7.4 W m^{-2}. For vertical slopes facing south, the error was 12 W m^{-2} for both Golden and Eugene. Values for E for south-facing slopes were close to 1 (ranging from 0.955 to 0.998), indicating good performance of the model for all inclinations at both locations. With regard to the modified index, d_i, values for south-facing slopes ranged from 0.93 to 0.96 at Golden and from 0.90 to 0.98 at Eugene. This indicates that the procedure was able to accurately estimate incoming solar radiation on south facing surfaces, given measured R_S on a horizontal surface.

Translated R_S for north-facing vertical slopes had the highest absolute errors due to the relative small values of solar radiation received for this extreme condition. The modified index was relatively high for north-facing slopes at both Colorado (0.80) and Eugene (0.70); however, the value for E was only moderately good in Colorado (0.78) and was relatively poor in Eugene (0.41), indicating that the procedure performed marginally well

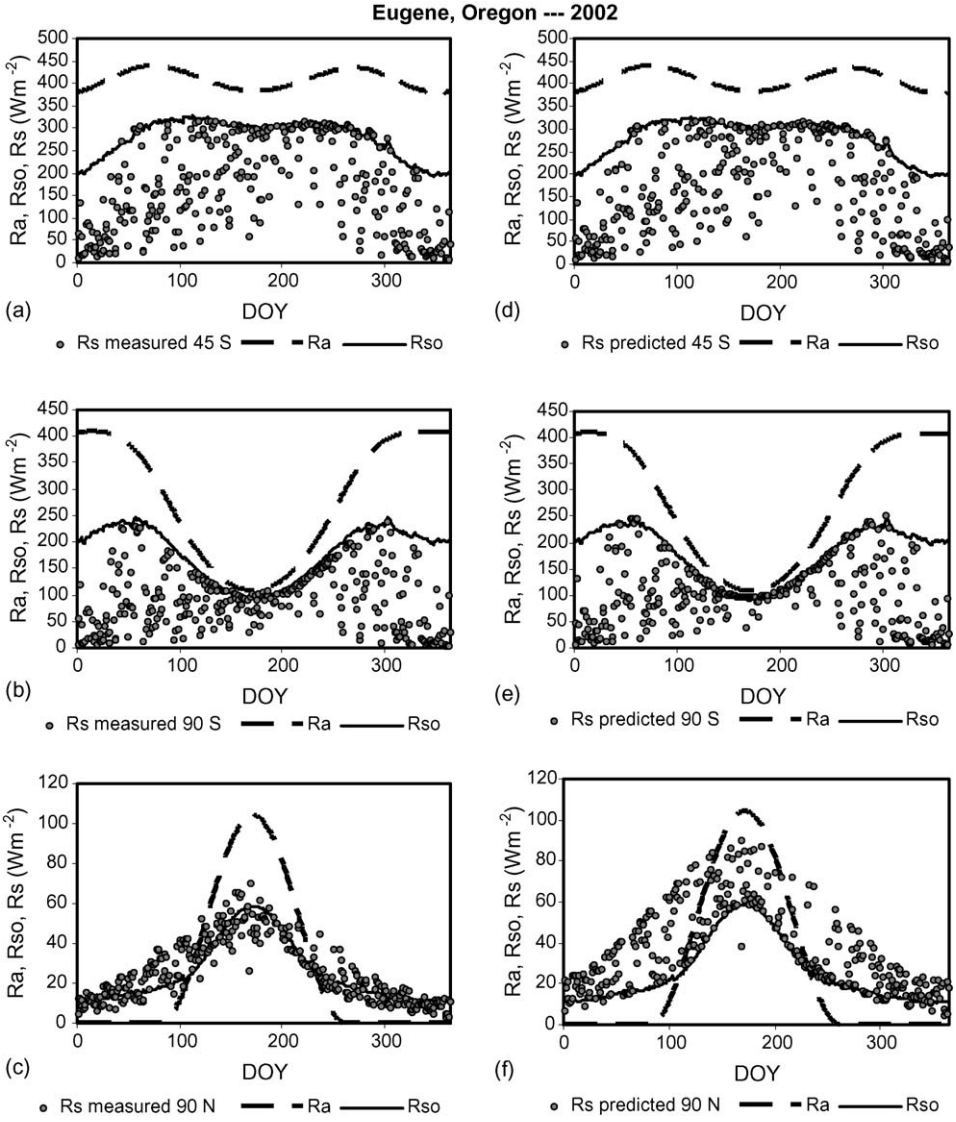

Fig. 3. Extraterrestrial solar radiation (R_a), clear-sky R_{so} envelope, and measured R_S at Eugene, Oregon, corresponding to slopes of (a) 45° (south-facing), (b) 90° (south-facing) and (c) 90° (north-facing) and associated predicted R_S for (d) 45° (south-facing), (e) 90° (south-facing) and (f) 90° (north-facing) slopes.

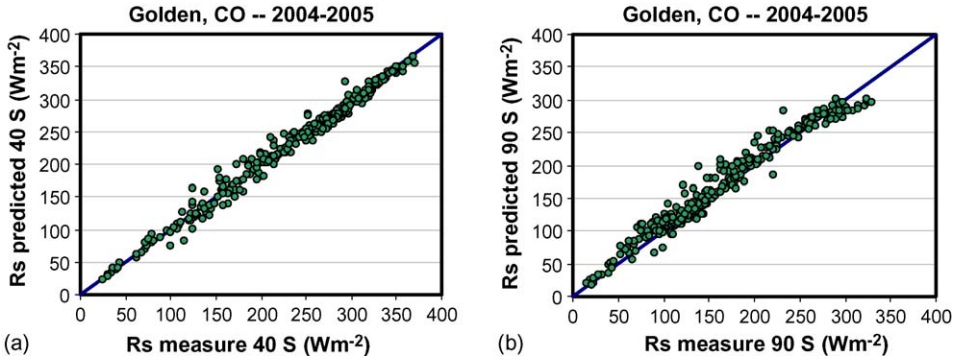

Fig. 4. Translated R_S vs. measured R_S at Golden, CO corresponding to south facing slopes of (a) 40° and (b) 90°.

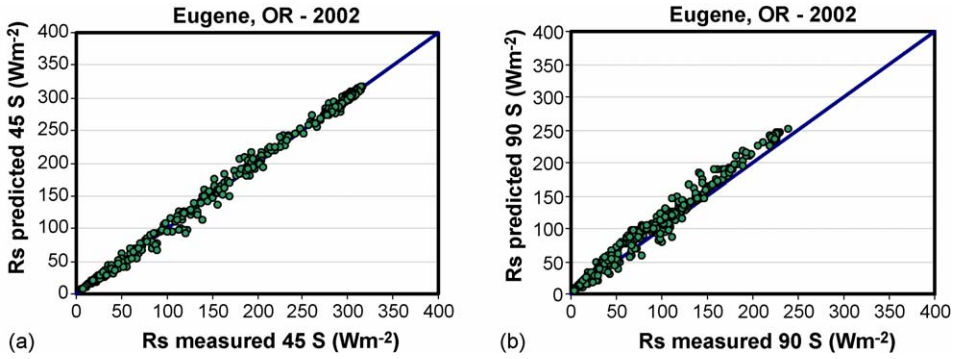

Fig. 5. Translated R_S vs. measured R_S at Eugene, OR corresponding to south facing slopes of (a) 45° and (b) 90°.

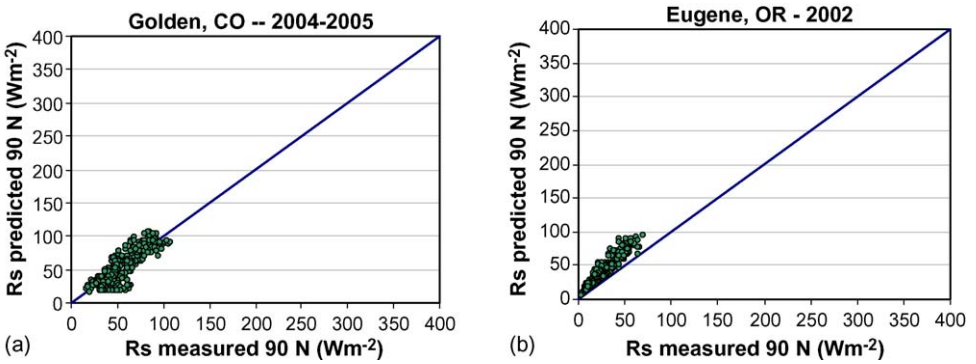

Fig. 6. Translated R_S vs. measured R_S at (a) Golden, CO and (b) Eugene, OR corresponding to north-facing slopes of 90°.

Table 4
Results of statistical analysis on solar radiation predictions

Station		Mean observed (W m^{-2})	S.D. observed (W m^{-2})	Mean predicted (W m^{-2})	S.D. predicted (W m^{-2})	R^2	RMSE (W m^{-2})	RMSE (%)	MAE (W m^{-2})	d_i	E
Golden, CO	40°S	234	81	233	80	0.982	14.9	6.4	7.39	0.962	0.986
	90°S	159	73	165	72	0.983	16.6	10.4	10.56	0.930	0.967
	90°N	55	21	51	26	0.849	15.3	27.8	11.77	0.801	0.775
Eugene, OR	30°S	173	109	173	110	0.999	5.5	3.2	3.81	0.984	0.998
	45°S	170	104	171	105	0.998	7.25	4.27	5.10	0.977	0.996
	90°S	93	60	103	64	0.989	14.0	15.1	11.5	0.902	0.955
	90°N	26	16	36	21	0.927	13.3	51.7	10.42	0.701	0.405

for these cases. On extreme north-facing slopes, the surface does not receive any direct beam radiation during a large portion of the year, so that the predicted solar radiation is only diffuse radiation, which is the more difficult solar component to estimate. During spring and summer, steep north-facing slopes received direct beam radiation during two separate periods during the day.

7. Conclusions

We have presented a procedure to analytically integrate extraterrestrial radiation during 24-h periods that can be applied to all combinations of latitude, slope and aspect having gradual to moderate terrain roughness. The developed analytical extraterrestrial radiation component is combined with general algorithms that consider impacts of atmospheric transmissivity and slope on direct beam, diffuse and reflected radiation to develop clear sky solar radiation curves that should generally need no local calibration. The procedures are further used to translate global solar radiation measurements from horizontal surfaces to nearby slopes. New developments reported here include a detailed procedure for determining integration limits for the analytical

solution that applies to all combinations of slope, aspect and latitude, including steep polar facing slopes where the sun may appear twice per day. Other developments include an improved function describing the reduction in hemispherical diffuse radiation with slope and adjustment of mean daily beam transmissivity using a weighted mean daily solar elevation. Simulated clear sky solar radiation envelope curves and translated measured solar radiation compared well with measurements from two locations in the U.S. over a range of slope and aspect.

Acknowledgements

We wish to acknowledge data provided by the University of Oregon solar radiation monitoring laboratory and the National Renewable Energy Laboratory at Golden, Colorado that was available for free access via the web and was of very high quality. We wish to thank Dr. Frank Vignola of University of Oregon, for providing review of results and advice on application of Oregon data. We also wish to thank the reviewers of this manuscript whose suggestions added much to clarity. Funding for this study stemmed from NASA-Raytheon, University of Idaho Agricultural and Engineering Experiment Stations, USDA-CSREES and Sandia National Laboratories.

Appendix A. Refinement to integration limits in Eq. (4)

The following procedure for determining the appropriate integration limits is recommended for application where all possible combinations of slope, aspect and solar angle may occur, including situations where the sun may never rise over the surface during the day (extreme latitudes during winter), where the sun may never set (extreme latitudes during summer), when the sunrise time for horizontal surfaces occurs later than the sunrise predicted for an infinite slope, when sunset time for horizontal surfaces occurs before the sunset predicted for an infinite slope, and where the sun disappears from sight behind a steep slope during some part of the day, but then reappears before final setting. The following steps A–D are followed:

A.1. Step A. Sunset (ω_S) and sunrise ($-\omega_S$) angles for horizontal slopes

Angles ω_S and $-\omega_S$ are used to constrain possible values for $\omega_{1_{24}}$ and $\omega_{2_{24}}$. Before calculating ω_S, however, the user must insure that the sun does rise and that it does set. Otherwise numerical errors will occur.

For the northern hemisphere (and assuming a slope of infinite extent with the same curvature as the earth):

- If $\delta + \phi > \pi/2$ then the sun never sets and there are 24 h of daylight. In this case sunset time angle $\omega_S = \pi$ and sunrise time angle $-\omega_S = -\pi$ for assessing specific integration limits.
- If $\delta - \phi > \pi/2$ then the sun never rises and there are 24 h of night. In this case, $\omega_S = -\omega_S = 0$ (i.e., sunrise = sunset) and $R_{a_{24}} = 0$ and there will be no estimated beam radiation on any slope.

For the southern hemisphere:

- If $\delta + \phi < -\pi/2$ then the sun never sets and there are 24 h of daylight. In this case, $\omega_S = \pi$ and $-\omega_S = -\pi$ for assessing specific integration limits.
- If $\delta - \phi < -\pi/2$ then the sun never rises and there are 24 h of night. In this case, $\omega_S = -\omega_S = 0$ (i.e., sunrise = sunset) and $R_{a_{24}} = 0$ and there will be no estimated beam radiation on any slope.

After establishing values for ω_S and $-\omega_S$, one calculates $\cos(\theta_{\omega_S})$ and $\cos(\theta_{-\omega_S})$ using slope and aspect for the specific surface to produce cosines of potential solar incidence angles when $\omega = \omega_S$ (time of horizontal sunset) and $\omega = -\omega_S$ (time of horizontal sunrise). These values are used during testing in steps B and C that follow. Fig. A1 shows a flow chart of calculations and conditionals described in step B for determining the actual sunrise limit. Step C follows a similar, and essentially mirror image of the process of step B.

A.2. Step B. Determine the beginning integration limit ($\omega_{1_{24}}$) representing the initial incidence of the center of the solar beam on the slope

i. Calculate $\sin(\omega_1)$ from (13a) and apply limits so that $-1 \leq \sin(\omega_1) \leq 1$.
ii. Solve for ω_1.
iii. Calculate $\cos(\theta_{\omega_1})$ using (3) or (14) for the value ω_1 from step ii.
iv. If $\cos(\theta_{-\omega_S}) \leq \cos(\theta_{\omega_1}) < 0.001$, then the value found for ω_1 from (13a) is valid and it correctly predicts the occurrence of sunrise on the slope as being after horizontal sunrise, and with the solar beam (disk) parallel to the slope and $\theta = -\pi/2$. This will generally occur for slopes facing away from the horizontal sunrise. Using the solution from (13a), $\omega_{1_{24}} = \omega_1$.

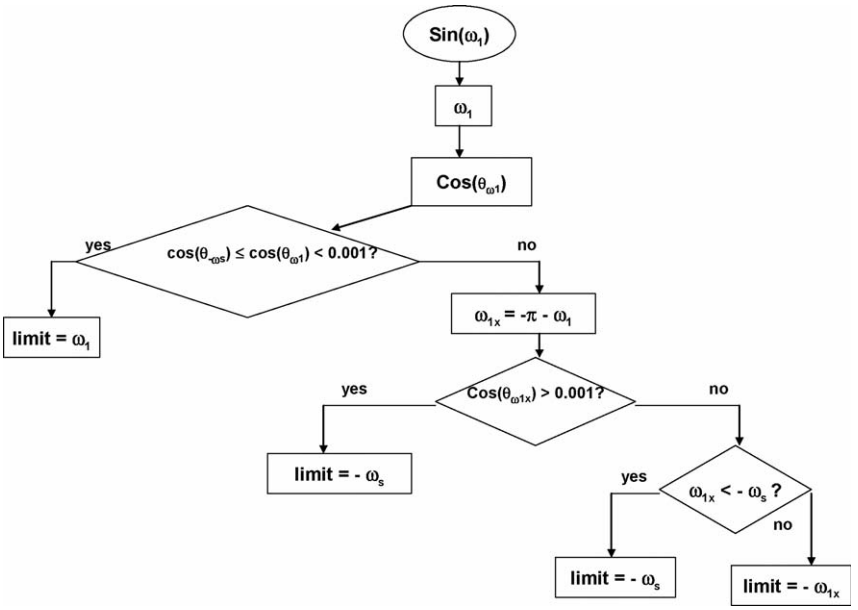

Fig. A1. Schematic showing flow of calculations and conditions for determining the beginning integration limit $\omega_{1_{24}}$ from step B.

v. Otherwise (if iv is false), sunrise for the slope may occur with the sun at some angle above the surface. This situation generally occurs for slopes facing the horizontal sunrise. In addition, a new candidate ω_{1_x} is evaluated that produces the same sine value as ω_1, and one calculates $\cos(\theta_{\omega_{1_x}})$ using (3) or (14) where the value for ω_1 from (13a) is corrected to $\omega_{1_x} = -\pi - \omega_1$.
   a. If $\cos(\theta_{\omega_{1_x}}) > 0.001$ then the lower limit of the integration is at the sunrise hour (as computed for a horizontal surface), and $\omega_{1_{24}} = -\omega_S$.
   b. If $\cos(\theta_{\omega_{1_x}}) \leq 0.001$ and $\omega_{1_x} \leq -\omega_S$ then the lower limit of the integration is at the sunrise hour (as computed for a horizontal surface), and $\omega_{1_{24}} = -\omega_S$.
   c. If $\cos(\theta_{\omega_{1_x}}) \leq 0.001$ and $\omega_{1_x} > -\omega_S$ then the sunrise on the slope occurs after horizontal sunrise, and the value for ω_{1_x} (where $\omega_{1_x} = -\pi - \omega_1$) is the correct and viable value for $\omega_{1_{24}}$, so that $\omega_{1_{24}} = -\pi - \omega_1$ where ω_1 is from (13a), with limits $-1 \leq \sin(\omega_1) \leq 1$ applied.

vi. At the conclusion of the calculation of $\omega_{1_{24}}$, $\omega_{1_{24}}$ is compared against $-\omega_S$ to insure that $\omega_{1_{24}} \geq -\omega_S$. This will prevent a northeast-facing slope (in the northern hemisphere) from "seeing" the sun through a transparent earth before the earth rises above the flat horizon. If $\omega_{1_{24}} < -\omega_S$ then $\omega_{1_{24}}$ is set to $\omega_{1_{24}} = -\omega s$.

vii. The value for $\omega_{1_{24}}$ resulting from steps i through vi can be used as the lower integration limit in Eqs. (5) and (6). This value is, however, subject to further limitations imposed under step D below to insure numerical stability.

A.3. Step C. Determine the ending integration limit ($\omega_{2_{24}}$) representing the final incidence of the center of the solar beam on the slope

i. Calculate $\sin(\omega_2)$ from (13b) and apply limits so that $-1 \leq \sin(\omega_2) \leq 1$.
ii. Solve for ω_2.
iii. Calculate $\cos(\theta_{\omega_2})$ using (3) or (14) from the value ω_2 from step ii.
iv. If $\cos(\theta_{\omega_S}) \leq \cos(\theta_{\omega_2}) < 0.001$, then the value found for ω_2 from (13b) is valid and it correctly predicts the occurrence of sunset on the slope as being before horizontal sunset, and with the solar beam (disk) parallel to the slope and $\theta = \pi/2$. This will generally occur for slopes facing away from the horizontal sunset. Using the solution from (13b), $\omega_{2_{24}} = \omega_2$.
v. Otherwise (if iv is false), sunset for the slope may occur with the sun at some angle above the surface. This situation generally occurs for slopes facing the horizontal sunset. In addition, a new candidate ω_{2_x} is evaluated that produces the same sine value as ω_2, and one calculates $\cos(\theta_{\omega_{2_x}})$ using (3) or (14) where the value for ω_2 from (13b) is corrected to $\omega_{2_x} = \pi - \omega_2$.
   a. If $\cos(\theta_{\omega_{2_x}}) > 0.001$ then the upper limit of the integration is at the sunset hour (as computed for a horizontal surface), and $\omega_{2_{24}} = \omega_S$.

b. If $\cos(\theta_{\omega_{2x}}) < = 0.001$ and $\omega_{1_x} \geq \omega_S$ then the upper limit of the integration is at the sunset hour (as computed for a horizontal surface), and $\omega_{2_{24}} = \omega_S$.
c. If $\cos(\theta_{\omega_{2x}}) \leq 0.001$ and $\omega_{2_x} < \omega_S$ then the sunset on the slope occurs before horizontal sunrise, and the value for ω_{2_x} (where $\omega_{2_x} = \pi - \omega_2$) is the correct and viable value for $\omega_{2_{24}}$, so that $\omega_{2_{24}} = \pi - \omega_2$, where ω_2 is from (13b), with limits $-1 \leq \sin(\omega_2) \leq 1$ applied.

vi. At the conclusion of the calculation of $\omega_{2_{24}}$, $\omega_{2_{24}}$ is compared against ω_S to insure that $\omega_{2_{24}} \leq \omega_S$. This will prevent a northwest-facing slope (in the northern hemisphere) from "seeing" the sun through a transparent earth after the earth sets below the flat horizon. If $\omega_{2_{24}} > \omega_S$ then $\omega_{2_{24}}$ is set to $\omega_{2_{24}} = \omega_S$.
vii. The value for $\omega_{2_{24}}$ resulting from steps i through vi can be used as the upper integration limit in Eqs. (5) and (6). This value is, however, subject to further limitations imposed under step D below to insure numerical stability.

A.4. Step D. Additional limits on $\omega_{1_{24}}$ and $\omega_{2_{24}}$ for numerical stability and twice per day periods of sun

In all cases, additional conditions are evaluated for the values of $\omega_{1_{24}}$ and $\omega_{2_{24}}$ determined from steps B and C to insure numerical stability of computations. Situations of numerical instability occur when slopes are steep and northerly facing in northern latitudes or southerly facing in southern latitudes so that the slope may be shaded during all or portions of the day:

i. The argument of the quadratic function in (13a) and (13b) must be limited to >0 for numerical stability. Therefore, if the argument is 0 or less, it is set equal to 0.0001.
ii. The value $\omega_{1_{24}}$ must be $\leq \omega_{2_{24}}$ (i.e., sunrise occurs before sunset). If $\omega_{2_{24}} < \omega_{1_{24}}$ then $\omega_{1_{24}} = \omega_{2_{24}}$ (i.e., no direct beam during the day). The incidence of calculated $\omega_{1_{24}} > \omega_{2_{24}}$ indicates that the slope is always shaded.
iii. The values for $\sin(\omega_1)$ and $\sin(\omega_2)$ from (13a) and (13b) must be within the intervals $-1 \leq \sin(\omega_1) \leq 1$ and $-1 \leq \sin(\omega_2) \leq 1$ for numerical validity before computing the arcsine functions (in steps ii under B and C). If the $\sin(\omega_1)$ or $\sin(\omega_2)$ are outside the limits of the interval (i.e., −1 and 1), then they are set equal to the limit.
iv. Two separate periods of beam radiation within a day. The integration of Eq. (5) and application of Eq. (6) presumes that there is a single, continuous daylight (direct beam) period during the day. In areas having steep slopes away from the sun, one must identify situations where the sun beam strikes the surface during two separate portions of the day. This situation can occur on relatively steep slopes facing away from the noontime sun during summer. In these situations, the slope may see the sun at sunrise, but then have the sun disappear behind the slope during midday, and then reappear before final sunset. These types of integration limits have not been reported elsewhere.To test whether a situation of two periods of direct beam radiation can potentially occur, Eq. (7) is solved, and if true ($\sin s > \sin\phi \cos\delta + \cos\phi \sin\delta$) then the slope exceeds the solar angle at solar noon and the possibility exists for two periods of direct beam radiation.

Therefore, the following sequence of conditionals should be applied to determine whether midday shading does occur so that two sets of integrations can be calculated and applied.

To identify situations where the sun beam strikes the surface during two separate portions of the day, four integration limits for (5) need to be defined and quantified:

a. $\omega_{1_{24}}$ the time angle when the center of the solar disk strikes the surface the first time.
b. $\omega_{2_{24b}}$ the time angle when the center of the solar disk disappears the first time.
c. $\omega_{1_{24b}}$ the time angle when the center of the solar disk reappears over the surface.
d. $\omega_{2_{24}}$ the time angle when the center of the solar disk disappears (sets) for the second (and last) time.

The following procedure quantifies these four integration limits and is applied when ($\sin s > \sin\phi \cos\delta + \cos\phi \sin\delta$):

a. $\omega_{1_{24}}$ and $\omega_{2_{24}}$ are calculated as described under steps B and C and limits are checked as described under steps D i–iii.
b. The candidates for intermediate integration limits $\omega_{2_{24b}}$, and $\omega_{1_{24b}}$ are:

$$\sin(A) = \frac{ac + b\sqrt{b^2 + c^2 - a^2}}{b^2 + c^2} \tag{44a}$$

$$\sin(B) = \frac{ac - b\sqrt{b^2 + c^2 - a^2}}{b^2 + c^2} \tag{44b}$$

where a, b, and c are defined in Eq. (11a)–(11c). Eq. (44a) is equivalent to (13b) listed earlier and

(44b) is equivalent to (13a), where angles A and B are temporary variables to be solved.

c. The values for $\sin(A)$ and $\sin(B)$ are limited to $-1 \le \sin(A) \le 1$ and $-1 \le \sin(B) \le 1$ before conversion to values A and B.

d. The candidates for $\omega_{2_{24b}}$ and $\omega_{1_{24b}}$ are solved as:

$$\omega_{2_{24b}} = \min(A, B) \tag{45}$$

$$\omega_{1_{24b}} = \max(A, B) \tag{46}$$

The predictions for $\omega_{2_{24b}}$ and $\omega_{1_{24b}}$ are preliminary and may need adjustment to compensate for the occurrence of two unique values for $\omega_{2_{24b}}$ and for $\omega_{1_{24b}}$, given values for $\sin(A)$ and $\sin(B)$. Therefore, a process similar to that used under steps ii–iv of steps B and C is applied. This process applies Eq. (3) or its simplified equivalent (14) to solve for $\cos(\theta_{\omega_{2_b}})$ and $\cos(\theta_{\omega_{1_b}})$ where $\cos(\theta_{\omega_{2_b}})$ is the solution from (3) or (14) for $\omega = \omega_{2_{24b}}$ and $\cos(\theta_{\omega_{1_b}})$ is the solution from (3) or (14) for $\omega = \omega_{1_{24b}}$. The values for $\omega_{2_{24b}}$ and $\omega_{1_{24b}}$ are then modified according to the outcome for $\cos(\theta_{\omega_{2_b}})$ and $\cos(\theta_{\omega_{1_b}})$, as discussed in the following paragraph.

e. Eq. (14) is applied to parameters $\omega_{2_{24b}}$ and $\omega_{1_{24b}}$ to calculate incidence angles:

$$\cos(\theta_{\omega_{2b}}) = -a + b\cos(\omega_{2_{24b}}) + c\sin(\omega_{2_{24b}}) \tag{47a}$$

$$\cos(\theta_{\omega_{1b}}) = -a + b\cos(\omega_{1_{24b}}) + c\sin(\omega_{1_{24b}}) \tag{47b}$$

where a, b, and c are constants for a given day, latitude, slope and slope azimuth and are defined in (11a)–(11c). The values for $\cos(\theta_{\omega_{2b}})$ and $\cos(\theta_{\omega_{1b}})$ from (47a) and (47b) are evaluated using the following conditionals:

$$\text{If } \cos(\theta_{\omega_{2b}}) < -0.001 \text{ or } \cos(\theta_{\omega_{2b}}) > 0.001 \text{ then } \omega_{2_{24b}} = -\pi - \omega_{2_{24b}} \tag{48a}$$

and

$$\text{If } \cos(\theta_{\omega_{1b}}) < -0.001 \text{ or } \cos(\theta_{\omega_{1b}}) > 0.001 \text{ then } \omega_{1_{24b}} = \pi - \omega_{1_{24b}} \tag{48b}$$

where $\omega_{2_{24b}}$ and $\omega_{1_{24b}}$ are the values that were used in (20).

f. In addition, the following constraints are imposed on final values for $\omega_{2_{24b}}$ and $\omega_{1_{24b}}$:

$$\omega_{2_{24b}} \ge \omega_{1_{24}} \tag{49a}$$

$$\omega_{1_{24b}} \le \omega_{2_{24}} \tag{49b}$$

These two constraints are used in two ways. First, they are used to limit the values for $\omega_{2_{24b}}$ and $\omega_{1_{24b}}$ before application of (50) and (50) below. Secondly, and as important, they can be used as an initial "filter" to determine whether there is only a single period of beam radiation occurring during the day, so that the following (50) does not need to be computed. This can improve computational efficiency.

g. Therefore, if either of the above constraints ((49a) and (49b)) are false, i.e., if $\omega_{2_{24b}} < \omega_{1_{24}}$ or if $\omega_{1_{24b}} < \omega_{2_{24}}$ then there is only a single beam period for the day and application of (50) and (51) is not required. However, if it is convenient to apply (50) and (51) for all pixels, for example during a spreadsheet or other application, then it is necessary to constrain $\omega_{2_{24b}}$ and $\omega_{1_{24b}}$ as noted by (49a) and (49b).

h. Satisfaction of constraints (49a) and (49b) does not necessarily indicate two periods of beam radiation during a day. To verify the condition where the day is broken into two separate periods of beam radiation, Eq. (5) (the integration of $\cos(\theta)$) is applied using the integration limits of $\omega_{2_{24b}}$ to $\omega_{1_{24b}}$ (after application of constraints of (49a) and (49b)). This is the period where the sunbeam is potentially blocked by the slope. The integration for this period is:

$$\begin{aligned} X &= \int_{\omega_{2_{24b}}}^{\omega_{1_{24b}}} \cos(\theta)\,\mathrm{d}\omega \\ &= \sin(\delta)\sin(\phi)\cos(s)(\omega_{1_{24b}} - \omega_{2_{24b}}) \\ &\quad - \sin(\delta)\cos(\phi)\sin(s)\cos(\gamma)(\omega_{1_{24b}} - \omega_{2_{24b}}) \\ &\quad + \cos(\delta)\cos(\phi)\cos(s)(\sin(\omega_{1_{24b}}) - \sin(\omega_{2_{24b}})) \\ &\quad + \cos(\delta)\sin(\phi)\sin(s)\cos(\gamma) \\ &\quad \times (\sin(\omega_{1_{24b}}) - \sin(\omega_{2_{24b}})) \\ &\quad - \cos(\delta)\sin(s)\sin(\gamma)(\cos(\omega_{1_{24b}}) - \cos(\omega_{2_{24b}})) \end{aligned} \tag{50}$$

i. If $X < 0$, the sunbeam does disappear from view of the slope during the period $\omega_{2_{24b}}$ to $\omega_{1_{24b}}$ and $R_{a_{24}}$ is then computed by summing the integration of (5) for the two periods separated by $\omega_{2_{24b}}$ and $\omega_{1_{24b}}$:

$$R_{a_{24}} = \frac{G_{sc}}{d^2}\left[\int_{\omega_{1_{24}}}^{\omega_{2_{24b}}} \cos(\theta)\,\mathrm{d}\omega + \int_{\omega_{1_{24b}}}^{\omega_{2_{24}}} \cos(\theta)\,\mathrm{d}\omega\right] \tag{51}$$

j. Otherwise, if X from (50) is ≥ 0, then the sunbeam is visible during a single portion of the day, only, and the single integration of (5) is carried out

using the integration limits $\omega_{1_{24}}$ and $\omega_{2_{24}}$ as in Eq. (6).

Appendix B. Equations used for statistical analysis

The following equations for statistical error parameters follow Legates and McCabe (1999):

a. Mean absolute error (MAE):

$$\mathrm{MAE} = \frac{\sum_{i=1}^{N} |O_i - P_i|}{N} \tag{52}$$

where O and P are observed and predicted values, N is the number of observations, and MAE is the mean absolute error expressed in the same units of O and P. MAE describes mean absolute difference between model observations and simulations in units of the variable.

b. Modified index of agreement (d_i):

$$d_i = 1.0 - \left(\frac{\sum_{i=1}^{N} (O_i - P_i)}{\sum_{i=1}^{N} (|P_i - \bar{O}| + |O_i - \bar{O}|)} \right) \tag{53}$$

where d_i ranges between 0 and 1.0. Higher index values represent superior performance of the model.

c. Coefficient of efficiency (E):

$$E = 1.0 - \left(\frac{\sum_{i=1}^{N} (O_i - P_i)^2}{\sum_{i=1}^{N} (O_i - \bar{O})^2} \right) \tag{54}$$

Physically, E is the ratio of the mean square error to the variance in the observed data, subtracted from unity. The coefficient of efficient (E) ranges from minus infinity to 1.0, where higher values indicate better performance. A value of zero indicates that the observed mean value is as good a predictor as the model, while negative values indicate that the observed mean is a better predictor than the model (Legates and McCabe, 1999).

References

Allen, R.G., 1996. Assessing integrity of weather data for use in reference evapotranspiration estimation. J. Irrigat. Drain. Eng., ASCE 122 (2), 97–106.

ASCE EWRI, 2005. The ASCE Standardized Reference Evapotranspiration Equation. Environmental and Water Resources Institute (EWRI) of the American Society of Civil Engineers Task Committee on Standardization of Reference Evapotranspiration Calculation, ASCE, Washington, DC, p. 190. http://www.kimberly.uidaho.edu/water/asceewri/.

Boes, E.C., 1981. Fundamentals of solar radiation. In: Kreider, J.F., Kreith, F. (Ed.), Solar Energy Handbook. p. 2-1-2-78 (Chapter 2).

Brutsaert, W., 1982. Evaporation into the Atmosphere. D. Reidel Publishing Co., Dordrecht, Holland, p. 300.

Collares-Pereira, M., Rabl, A., 1979. The average distribution of solar radiation correlations between diffuse and hemispherical and between daily and hourly insolation values. Solar Energy 22, 155–164.

Diez, M., De Miguel, A., Bilbao, J., 2005. Measurements and comparison of diffuse solar irradiance models on inclined surfaces in Valladolid (Spain). Energy Conver. Manage. 46, 2075–2092.

Dubayah, R., Dozier, J., Davis, F.W., 1990. Topographic distribution of clear-sky radiation over the Konza Prairie, Kansas. Water Resour. Res. 26, 679–690.

Duffie, J.A., Beckman, W.A., 1980. Solar Engineering of Thermal Process, 1st ed. John Wiley and Sons, NY.

Duffie, J.A., Beckman, W.A., 1991. Solar Engineering of Thermal Process, 2nd ed. John Wiley and Sons, NY.

Flint, A., Childs, S.W., 1987. Calculation of solar radiation in mountains terrain. Agric. Forest Meteorol. 40, 233–249.

Fu, P., Rich, P.M., 1999. Design and implementation of the solar analyst: an ArcView extension for modeling solar radiation at landscape scales. Proceedings of the 19th Annual ESRI User Conference, San Diego, USA, http://www.esri.com/library/userconf/proc99/proceed/papers/pap867/p867.htm.

Garner, B.J., Ohmura, A., 1968. A method for calculating direct shortwave radiation income of slopes. J. Appl. Meteorol. 7, 796–800.

Garrison, J.D., Adler, G.P., 1990. Estimation of precipitable water over the United States for application to the division of solar radiation into its direct and diffuse components. Solar Energy 44 (4), 225–241.

Hay, J.E., 1979. Calculation of monthly mean solar radiation for horizontal and inclined surfaces. Solar Energy 23, 301–307.

Hay, J.E., 1993. Calculating solar radiation for inclined surfaces: practical approaches. Renew. Energy 3 (4/5), 373–380.

Ineichen, P., Guisan, O., Perez, R., 1990. Ground-reflected radiation and albedo. Solar Energy 44 (4), 207–214.

Ineichen, P., Perez, R., Seals, R., 1987. The importance of correct albedo determination for adequately modeling energy received by tilted surfaces. Solar Energy 39 (4), 301–305.

Klein, S.A., 1977. Calculation of monthly average insolatino on tilted surfaces. Solar Energy 19, 325–329.

Legates, D.R., McCabe Jr., G.J., 1999. Evaluating the use of "goodness-of-fit" measures in hydrologic and hydroclimatic model validation. Water Resour. Res. 35, 233–241.

Liu, Y.H., Jordan, R., 1960. The interrelationship and characteristic distribution of direct, diffuse, and total solar radiation. Solar Energy 4 (3), 1–19.

Li, D.W., Lam, J., Lau, C., 2002. A new approach for predicting vertical global solar irradiance. Renew. Energy 25, 591–606.

Majumdar, N.C., Mathur, B.L., Kaushik, S.B., 1972. Prediction of direct solar radiation for low atmospheric turbidity. Solar Energy 13, 383–394.

Marks, D., Dozier, J., Davis, R.E., 1979. A clear-sky longwave radiation model for remote alpine areas. Archiv fur Meteorologie, Geophysik und Bioklimatologie, Series B 27 (3), 159–187.

Nijmeh, S., Mamlook, R., 2000. Testing of two models for computing global solar radiation on tilted surfaces. Renew. Energy 20, 75–81.

NOAA-SURFRAD, 2006. NOAA-SURFRAD data repository, the Surface Radiation Research Branch website. http://www.srrb.noaa.gov/surfrad/desrock.html (accessed February 2006).

Perez, R., Ineiche, P., Seals, R., Michalsky, J., Steward, R., 1990. Modeling daylight availability and irradiance components from direct and global irradiance. Solar Energy 44, 271–289.

Reindl, D.T., Beckman, W.A., Duffie, J.A., 1990. Evaluation of hourly tilted surface radiation models. Solar Energy 45, 9–17.

Revfeim, K.J.A., 1978. A simple procedure for estimating global daily radiation on any surface. J. Appl. Meteorol. 17, 1126–1131.

Robledo, L., Soler, A., 1998. Modelling irradiance on inclined planes with an anisotropic model. Energy 23 (3), 193–201.

Swift, L.W., 1976. Algorithm for solar radiation on mountain slopes. Water Resour. Res. 12, 108–112.

Tian, Y.Q., Davies-Colley, R.J., Gong, P., Thorrold, B.W., 2001. Estimating solar radiation on slopes of arbitratry aspect. Short communication. Agric. Forest Meteorol. 109, 67–74.

Trezza, R., Allen, R.G., 2006. Procedure and calculation steps for solar radiation and reference evapotranspiration (ETo) on inclined surfaces. Appendix C of Sandia National Laboratories report Simulation of Net Infiltration for Present-Day and Potential Future Climates MDL-NBS-HS-000023 REV 01. University of Idaho Research and Extension Center.

University of Oregon, 2005. Pacific Northwest Solar Radiation Data book. Available at http://solardat.uoregon.edu/PacNWSolarRadiationDataBook.html.

Varley, M.J., Beven, K.J., Oliver, H.R., 1996. Modelling solar radiation in steeply sloping terrain. Int. J. Climatol. 16 (1), 93–104.

Vignola, F., McDaniels, D.K., 1986. Beam-global correlations in the Pacific Northwest. Solar Energy 36 (5), 409–418.

Zeroual, A., Ankrim, M., Wilkinson, A., 1996. The diffuse-global correlation: its application to estimating solar radiation on tilted surfaces in Marrakesh, Morocco. Renew. Energy 7, 1–13.